

Ring-shaped images as a result of nonuniform field emission from capped carbon nanotubes

L. D. Filip

University of Bucharest, Faculty of Physics, P.O. Box MG-11, Bucharest-Magurele 76900, Romania

D. Nicolaescu^{a)}

Nanoelectronics Research Institute, AIST, 1-1-1 Umezono, Tsukuba, Ibaraki 305-8568, Japan

M. Tanemura

Department of Environmental Technology, Nagoya Institute of Technology, Gokiso-cho, Showa-ku, Nagoya 466-8555, Japan

S. Kanemaru and J. Itoh

Nanoelectronics Research Institute, AIST, 1-1-1 Umezono, Tsukuba, Ibaraki 305-8568, Japan

(Received 8 October 2004; accepted 3 January 2005; published 6 April 2005)

A model for electron field emission from carbon nanotubes (CNTs) has been developed and modeling results are presented. The model assumes that for high emission currents, part of the electrons behave as quasifree. As a result, the spatial confinement quantization of their states appears, the tunneling field emission taking place from these states into the vacuum. The probability of finding an electron in a small axial interval is higher close to the CNT cylindrical body, while the extraction field is higher on the CNT hemispherical tip. These two opposite trends lead to enhancement of the CNT lateral field emission for higher extraction voltages. The model outlines the possibility of inhomogeneous electron field emission for very thin CNTs at high emission levels and the appearance of peculiar ring-shaped and/or spot-shaped field emission images, in accordance to available experimental observations. © 2005 American Vacuum Society.

[DOI: 10.1116/1.1864059]

I. INTRODUCTION

Carbon nanotubes (CNTs) are actively investigated for their field emission properties. Experimental results¹⁻⁸ have disclosed many peculiarities of CNT field electron emission. The field emission images on the anode plane usually show one central spot or small groups of spots that appear to be symmetrically arranged close to the center. However, for high fields/high temperature conditions, more complicated (FE) images comprising emission rings or auras surrounding the central emission spots may appear. Normally one might presume that such circular features could be assigned to some opened CNTs present in the film cathode. Nevertheless, there is strong evidence that ring images appear in the case of closed CNTs too.^{4,8} Conventional theoretical simulations^{9,10} consider that the electron emission proceeds from electronic states localized near the CNT apex, where the electric field has its highest values. This approach accounts for basic features of the CNT emission process but may not explain the appearance of peculiar ring-shaped field emission images.

In this article, a model for field emission from CNTs is developed. The model refers to a capped nanotube with cylindrical body and hemispherical cap. It is assumed that for high electric fields/high emission currents, part of the electrons behave as quasifree.^{11,12} As a result of the spatial confinement, quantization of their states appears and the tunnel-

ing field emission takes place from these states into the vacuum. The electron localization in the radial direction is considered so tight that the corresponding position parameter could be disregarded in the description of the electronic quantum state. As a consequence, the electron is regarded as a purely two-dimensional object evolving on a surface composed by a cylindrical body with a hemispherical termination. The electron is bound to this structure with some uniform potential energy $-W_0$. Thus, the Schrödinger equation for the single electron can be solved separately on the cylindrical and spherical parts of the structure and the corresponding solutions can be connected smoothly at the circular intersection of the two regions. Periodic boundary conditions are imposed to the solution on the cylindrical part. The requirement that the eigenvalues (energies) of the correspondent solutions on both regions be equal leads to selective relations to be satisfied by the related quantum numbers. As a consequence, many of the electronic states that are possible on the two regions when taken separately turn out to be forbidden for the capped nanotube. The selection of the possible electronic states under the aforementioned complex conditions is determined by the geometric parameters of the tube, namely, the ratio between its length and diameter. The occupation of the allowed one-electron states is considered as governed by the usual Fermi statistics. Together with the quantum probability of finding an electron in some specified area of the surface, this gives the electron distribution on the tube, which is one of the key factors determining the electron field emission from the CNT. Another key factor is the ap-

^{a)}Author to whom correspondence should be addressed; electronic mail: n-dan@aist.go.jp

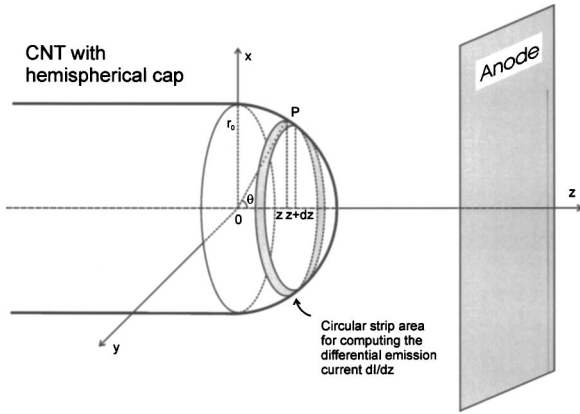


FIG. 1. Field emission configuration considered for the present theoretical analysis. The CNT has a cylindrical body and a hemispherical cap. For each infinitesimal circular strip area on the CNT cap of axial position z and width dz , a specific amount of available electrons and a local extraction field is considered.

plied extraction field. The probability of finding an electron in a small axial interval is higher close to or on the CNT cylindrical body, while the extraction field is higher on the CNT hemispherical tip. These two opposite trends lead to enhancement of the CNT lateral field emission for higher extraction voltages. As a result, for high field/high current conditions, nonuniform field emission images may appear, comprising brighter rings and darker central sites. The extraction field and the electron trajectories have been numerically computed using Simion¹³ for a nanotube-on-post diode configuration.

II. PHYSICAL MODEL

The model used in this article for the electron behavior on the CNT sheet follows roughly the lines developed in Ref. 11. Using a continuous one-particle approximation, the electron is considered as a quasifree object evolving on a strict two-dimensional manifold. The model takes into account a cylindrical sheet of length L , terminated smoothly by a hemisphere of the same diameter, as depicted in Fig. 1 (and not only the hemispherical cap¹¹). The tube has a radius r_0 and the z axis of the system of coordinates is chosen along its axis. The origin of the z axis is taken as an intersection with the cylinder-hemisphere common plane, its positive sense being toward the hemisphere tip. Convenient position parameters for the hemisphere are the azimuth angle φ and the relative coordinate $\zeta = z/r_0$, while for the cylindrical surface, φ and $\xi = z/L$ will be used. By setting an overall position-invariant electron potential energy $-W_0$ ($W_0 > 0$) (Ref. 11) on both the cylinder and the hemisphere, well-known procedures can be readily used to construct and solve the two-dimensional Schrödinger equation, separately in the two regions.¹²

Thus, the general solution on the hemisphere ($0 \leq \zeta \leq 1$), which remains finite on the tip, can be written as^{11,14,15}

$$u_{l,m}^s(\zeta, \varphi) = C \sqrt{\frac{(l+m)!}{(2l+1)(l-m)!}} P_{l,m}(\zeta) \Phi_m(\varphi), \quad (1)$$

where C is some undetermined constant, l and m are integers such that l is non-negative and $m = -l, -l+1, \dots, l$. The symbol $P_{l,m}(\zeta)$ stands for the associated Legendre function¹⁵ normalized on the interval $[0, 1]$ and

$$\Phi_m(\varphi) = \frac{1}{\sqrt{2\pi}} e^{im\varphi}. \quad (2)$$

The related allowed electron energies are

$$E_l = \frac{\hbar^2}{2m_0 r_0^2} l(l+1) - W_0. \quad (3)$$

On the cylindrical part of the manifold, the general solution reads

$$u^c(\xi, \varphi) = (A e^{i\Omega\xi} + B e^{-i\Omega\xi}) \Phi_m(\varphi), \quad (4)$$

where A and B are undetermined constants and

$$\Omega = \sqrt{\frac{2m_0 L^2}{\hbar^2} \left(E + W_0 - \frac{\hbar^2 m^2}{2m_0 r_0^2} \right)} \quad (5)$$

for $E > (\hbar^2 m^2)/(2m_0 L^2) - W_0$. As the electronic state should not change after a rotation with 2π around the z -axis, it follows that m takes integer values in Eq. (4), too.

The overall solution as well as its first derivatives should be continuous at the intersection of the two regions.¹⁴ Therefore, for every $\varphi \in [0, 2\pi]$, we may write

$$u_{l,m}^s(0, \varphi) = u^c(0, \varphi) \quad (6)$$

and

$$\frac{1}{r_0} \frac{\partial u_{l,m}^s}{\partial \zeta}(0, \varphi) = \frac{1}{L} \frac{\partial u^c}{\partial \xi}(0, \varphi). \quad (7)$$

It is quite clear that Eqs. (6) and (7) occur for the *same value of the energy* on the both sides of the equalities. That is, in Eq. (5) one should replace the value of the energy given by Eq. (3). Thus, Ω (and consequently u^c too) turns into a (l, m) -dependent quantity

$$\Omega_{l,m} = \frac{L}{r_0} \sqrt{l(l+1) - m^2}. \quad (8)$$

Also, Eq. (6) implies first that the values of m in the cylinder solution of Eq. (4) should be the same as those allowed for the hemisphere solution, namely, $m = -l, -l+1, \dots, l$, for every non-negative integer l .

It is worthy to note here that the form of Eq. (8) and the previous limitations in the ranges of l and m imposed by the necessary connection with the hemisphere solution actually rule out any nonoscillating solution on the cylinder sheet. For such a solution to exist it would be needed that $l(l+1) \leq m^2$, which leads to the trivial result $l=m=0$ only.

In addition to these general conclusions, Eqs. (6) and (7) allow also the computation of the constants A and B from Eq. (4) as multiples of the constant C of Eq. (1). Finally, C results from the overall normalization condition

$$\int_{-1}^0 \int_0^{2\pi} |u_{l,m}^c(\xi, \varphi)|^2 d\varphi d\xi + \int_0^1 \int_0^{2\pi} |u_{l,m}^s(\zeta, \varphi)|^2 d\varphi d\zeta = 1. \quad (9)$$

As the behavior of the associated Legendre functions and of their first derivatives at the connection point $\zeta=0$ differs upon the parity of the sum $l+m$,¹⁵ the final result for the quasifree electronic wave function naturally splits in two cases. Thus, for $l+m=\text{even integer}$, we get

$$\psi_l^m(z, \varphi) = \Phi_m(\varphi) \times \begin{cases} \frac{P_{l,m}(0)}{\sqrt{L \left[1 + \frac{1}{2} [P_{l,m}(0)]^2 \right]}} \cos \left[\frac{z}{r_0} \sqrt{l(l+1) - m^2} \right], & \text{for } -L \leq z \leq 0 \\ \frac{1}{\sqrt{r_0 \left[1 + \frac{1}{2} [P_{l,m}(0)]^2 \right]}} P_{l,m} \left(\frac{z}{r_0} \right), & \text{for } 0 \leq z \leq r_0 \end{cases} \quad (10)$$

and for the case $l+m=\text{odd integer}$, the result is

$$\psi_l^m(z, \varphi) = \Phi_m(\varphi) \times \begin{cases} \frac{P'_{l,m}(0)}{\sqrt{L \left[l(l+1) - m^2 + \frac{1}{2} [P'_{l,m}(0)]^2 \right]}} \sin \left[\frac{z}{r_0} \sqrt{l(l+1) - m^2} \right], & \text{for } -L \leq z \leq 0 \\ \frac{1}{\sqrt{r_0 \left[l(l+1) - m^2 + \frac{1}{2} [P'_{l,m}(0)]^2 \right]}} P_{l,m} \left(\frac{z}{r_0} \right), & \text{for } 0 \leq z \leq r_0. \end{cases} \quad (11)$$

Up to this point no boundary condition was questioned at the other end of the CNT model. In many situations this may be a contact to a substrate or a physical boundary whose properties are difficult to define. However, any supplementary condition imposed at this end will certainly enforce new restrictions on the allowed quasifree states labeled by l and m . Therefore, for convenience reasons, we take such supplementary constraints as being the (very usual in crystal physics) periodic boundary conditions

$$\psi_{l,m}(z, \varphi) = \psi_{l,m}(z + L, \varphi). \quad (12)$$

When applied to the wave functions in both cases of Eqs. (10) and (11), this condition leads to $\Omega_{l,m} = 2n\pi$, for $l+m = \text{even integer}$ and $\Omega_{l,m} = n\pi$, for $l+m = \text{odd integer}$, for any non-vanishing integer n . In other words, the supplementary constraint imposed by the new boundary condition on the values of l and m is that the quantity $(L/\pi r_0)^2 [l(l+1) - m^2]$ should be the *square of an even nonvanishing integer*, for $l+m = \text{even integer}$ and the *square of any nonvanishing integer*, for $l+m = \text{odd integer}$.

Following Ref. 11, Eqs. (10) and (11) may be used to define a probability density of the axial electron localization on the capped CNT:

$$\prod_l^m(z) = \int_0^{2\pi} |\Psi_l^m(z, \varphi)|^2 d\varphi. \quad (13)$$

This expression defines the probability of finding a

(l, m) -state electron in a circular strip area of extent dz , around the axial position z on the capped tube. By also taking into account the statistical occupancy of these states, one may readily define the axial density of the quasifree electrons on the CNT¹¹

$$\frac{dn_z^{\text{free}}}{dz} = \sum_{l=0}^{\infty} f(E_l) \sum_{m=-l}^l \prod_l^m(z), \quad (14)$$

where, for convenience,

$$f(E_l) = 2(2l+1) \left[1 + \exp \left(\frac{E_l}{k_B T} \right) \right]^{-1} \quad (15)$$

is the Fermi–Dirac function, corrected for the spin and m degeneracy.

The quantity defined in Eq. (14) is essentially what may be detected by scanning tunneling microscopy (STM) along longitudinal axes of real CNTs¹⁶ and thus allows direct comparison of the model predictions with related experimental data and extraction of useful information about the actual content of quasifree electrons on the CNT.

Another type of experimental investigation may be performed by field electron emission. In order to compute the field emission current due to the quasifree electrons on a capped CNT one should rely on some vacuum tunneling mechanism. Following the previous work of Ref. 11 we shall use the WKB approximation and write the tunneling probability from a specified position on the CNT as

$$D_l(z) = \exp \left[- \frac{4 \sqrt{2m_0} (\chi - E_1)^{3/2}}{3 \hbar e F(z)} \right], \quad (16)$$

where $F(z)$ is the local value of the applied field strength in some point z on the surface of the CNT and χ is the work function of the CNT taken as 4.7 eV.

The semiclassical approximation may not seem quite appropriate for the specific case of CNT field emission. Nevertheless, we will make use of its simplicity since the main purpose of this article is not to compute accurate field emission currents, but to outline field emission inhomogeneities observable in field emission imaging experiments, which are presumably due to the presence of quasifree electrons on CNTs.

The electronic states described by Eqs. (10) and (11) carry no radial current. Therefore the tunneling of an electron between such states and the states in the vacuum should be described in the framework of decay phenomena by using the semiclassical concept of attempt-to-escape rates^{17,18,11}

$$v_l^m = \frac{v_l^m}{2t}, \quad (17)$$

where t is so-called localization parameter and v_l^m is a characteristic velocity of the state (l, m) .¹⁸ From the classical point of view, in a plane perpendicular to the tube axis, the electron appears to rotate with the angular momentum $m\hbar$. Therefore, v_l^m could be taken as $|m|\hbar/m_0r_0$ and $2t$ would equal $2\pi r_0$. The attempt-to-escape rate could be thus written as $v_l^m = |m|\hbar/2\pi m_0r_0^2$. Nevertheless, one may observe that, while this expression is a reasonable estimate for the electron attempt-to-escape rate for each case with $m \neq 0$, it precludes the emission of nonrotating electrons, for which $m=0$. For this last situation, the form of the attempt-to-escape rate used in Ref. 11 will be adopted. Therefore, we may write

$$v_l^m = \begin{cases} \frac{\hbar \sqrt{l(l+1)}}{2m_0r_0^2}, & \text{for } m=0 \\ \frac{\hbar |m|}{2\pi m_0r_0^2}, & \text{for } m \neq 0. \end{cases} \quad (18)$$

By using Eqs. (13) and (15)–(17), we can now define the axial distribution of the emission current (i.e., the emission current from a CNT circular strip between the coordinates z and $z+dz$) as

$$\frac{dI}{dz}(z) = e \sum_{l=0}^{\infty} f(E_l) D_l(\zeta) \sum_{m=-l}^l v_l^m \prod_l(z). \quad (19)$$

This expression gives the emission current linked to every site on the CNT. Local fields and electron trajectory computations can be further used in order to derive field emission images projected on the anode plane.

III. ELECTRIC FIELD AND ELECTRON TRAJECTORIES COMPUTING

The electric field F_0 on a sharp emitter of radius r_0 (such as a needle in front of the anode plane) may be obtained using the empirical formula¹⁹

$$F_0 = \frac{V_a}{sr_0}, \quad (20)$$

where V_a is the anode voltage and s is a self-screening factor usually taken as 5.

However, in order to describe the field emission process taking place from different areas of the emitter, a more detailed approach is needed. The electric field distribution has been computed using the SIMION 3D 7.0 software package¹³ for a nanotube-on-post diode configuration. The nanotube-on-post arrangement corresponds to experimental situations where the CNT is grown on metallic “needles.” The length of the post (needle), taken as $h_p=6.25 \mu\text{m}$, is much larger than the CNT length $L=20 \text{ nm}$. As a result, the electric field F_0 on the CNT tip depends mostly on the CNT radius r_0 and anode voltage V_a but (for practical purposes) does not depend on the nanotube length L .

Several general considerations for using SIMION to model field emission devices are presented in Ref. 20. The program numerically solves the Laplace equation for the potential, the derivatives being approximated by finite differences using a lattice with constant mesh size. However, multiple instances¹³ are allowed. Instances are self-contained problems that are connected through common boundary conditions. Different instances may have different mesh step sizes, allowing one to model structures with fine details such as field emitters. Complex structural configurations could be precisely defined using geometry files. These two program features have been used in the present modeling approach. The first instance comprises the 16.25- μm -wide region between the anode and cathode electrodes (of which $h_p=6.25 \mu\text{m}$ is the post height and $d=10 \mu\text{m}$ is the CNT tip to anode plane spacing), the lattice step size being $s_1=6.25 \text{ nm}$. The second instance, showing in Fig. 2, models the 150-nm-wide region containing the CNT tip and body, the lattice step size being $s_2=0.1 \text{ nm}$. Finally, the region close to the CNT tip, shown in Fig. 3, is modeled by the “Instance 3” for which the lattice step is $s_3=s_2/64 \text{ nm}$.

The computed electric field for several CNT radii is shown in Fig. 4, the abscissa coordinate being the normalized axial position $\zeta=z/r_0$. The anode potential considered for computation is $V_a=100 \text{ V}$, but field values are scalable with V_a . However, the field emitted electrons have trajectories which depend on the applied potential, although the changes are significant only for high fields. In Fig. 5, the radial position of the electron impact point on the anode plane is plotted as a function of its departure (normalized axial) position $\zeta=z/r_0$.

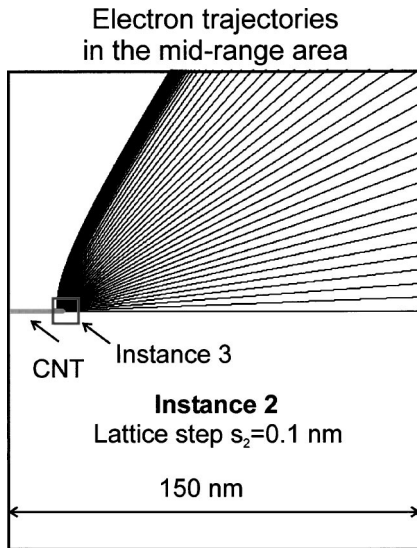


FIG. 2. Electron trajectories for the midrange region [“Instance 2” for computing the electric field with Simion (Ref. 13)].

IV. MODELING RESULTS AND DISCUSSIONS

The physical model presented above is devoted to the behavior of the very mobile electrons on the CNT sheet. These electrons are described as quasifree and found to move under the quantum constraints imposed by the specific spatial confinement. It may be asserted that the behavior of the quasifree electrons strongly influences both the charge transport in CNTs and their field emission properties. The present study reveals that a CNT should not be treated simply as a pipe for electrons (even if the lower dimensionality is taken into account). Rather, the CNT should be considered as a “two-dimensional resonant structure,” which may enforce various selective constraints for the electronic waves. Recent STM explorations of local electron density on CNTs¹⁶ seem to sustain such a viewpoint. In order to make a comparison to our model’s predictions we have computed the axial elec-

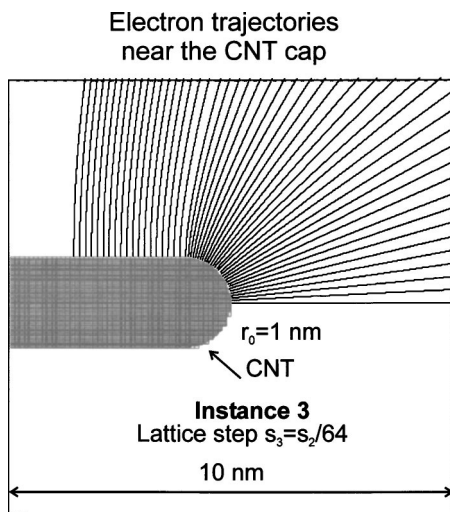


FIG. 3. Electron trajectories for the region close to the CNT cap [“Instance 3” for computing the electric field with Simion (Ref. 13)].

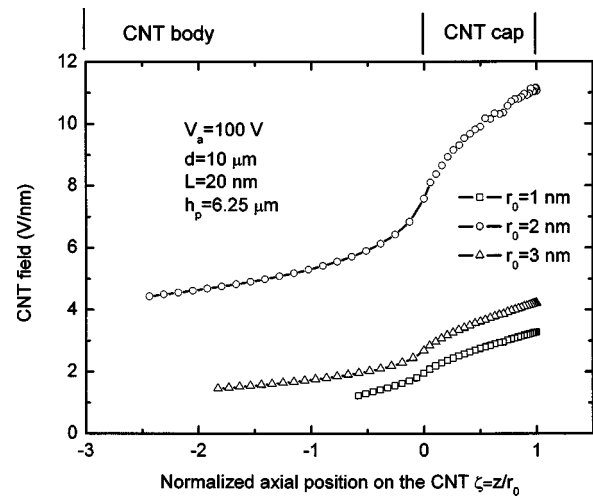


FIG. 4. Electric field on the CNT (cap and body) as function of the normalized axial position on the CNT $\zeta = z/r_0$.

tron density through Eq. (14). Some results, obtained for two CNT diameters and for two values of the parameter W_0 (which is strictly related to the quasifree electronic content¹²) are displayed in Fig. 6. There is a visible similarity between these diagrams and the STM measurements of Ref. 16. While the current explanation of such images relies entirely on the tight binding electronic model¹⁶ and are viewed as a projection of the intimate atomic structure of the CNT, the similarity with the diagrams of Fig. 6 at least indicates that the contribution of the quasifree electrons to the net experimental results should not be ruled out. As might have been expected, there is a high sensitivity of the axial quasifree electron distribution to both the tube dimensions and its content of quasifree electrons. By taking special care to dissociate the signals produced by the tightly bound electrons, such features might obviously be speculated for future intensive exploration of CNTs through STM studies. Therefore, it may be expected that further work in this direction (comprising both more specialized measurements and related model com-

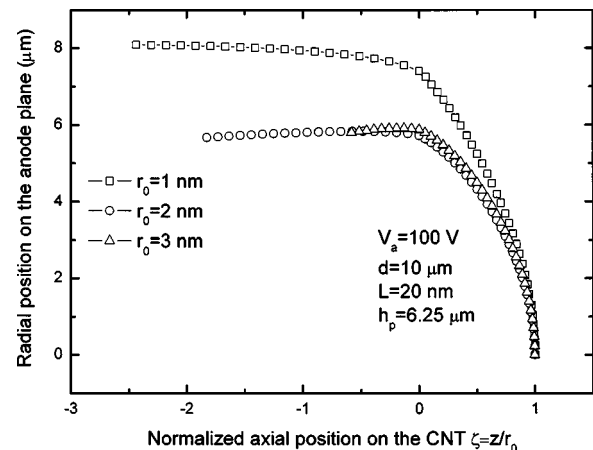


FIG. 5. Radial coordinate of the electron impact point on the anode plane as function of its departure (normalized axial) position $\zeta = z/r_0$.

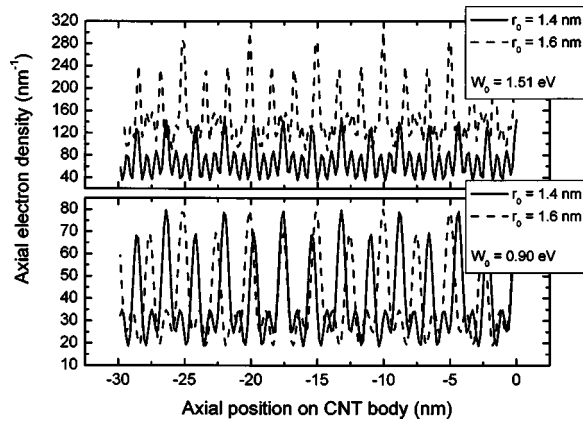


FIG. 6. Computed axial electron density through Eq. (14), obtained for two CNT diameters and for two values of the parameter W_0 .

putations with more adequate boundary conditions) could bring valuable insight to the field of electron transport in such nanostructures as CNTs.

As it is already well known, the electron field emission from CNTs provides an alternative opportunity to explore their electronic structure. In particular, the techniques of field emission imaging^{1-3,5} clearly reveal that the electrons are not homogeneously emitted from the CNT's cap. In many situations the images are consistent with the field emission from the atomic sites on the CNT's cap, where the tightly bounded electrons tend to concentrate and where high local field enhancement occur.^{2,9,10} Even configuration changes of the CNT cap structure can be visualized in this way.^{1,2} Nevertheless, other CNT field emission imaging effects remain unexplained in such a discrete model. Thus, one may frequently observe the formation of homogeneous rings surrounding the field emission image from a CNT.²⁻⁵ Also, singular homogeneous emission spots produced by individual CNTs appear together with ring images in experiments performed on broader area of a CNT film.^{3,5} Moreover, the density of the emission sites in CNT films seems to be usually too low to be assigned to the electrostatic screening of the local extraction field only.^{3,5,21} These observations lead to the hypothesis that quasifree electrons may also have their contribution to the field emission from CNTs. In order to support this assumption we applied our continuous model to single CNTs of various configurations and obtained the final field emission image on an anode placed perpendicularly on the CNT axis. As pointed out in Ref. 11, the extraction field value on the CNT surface is not expected to be uniform. In fact there is a steep (two-three times) decrease of the field from the CNT's tip toward its body (see Fig. 4). In a normal field emitter, this should give rise to an intense current from the tip and an even steeper decrease of the emission toward the body. Nevertheless, as shown in the results depicted in Fig. 6, the quantum behavior of the quasifree electrons in such a structure allows a nonuniform distribution of the electron density on the CNT, which convolutes with the tunneling probability into the vacuum. From the competition of these two factors, a much more complicated axial current distribu-

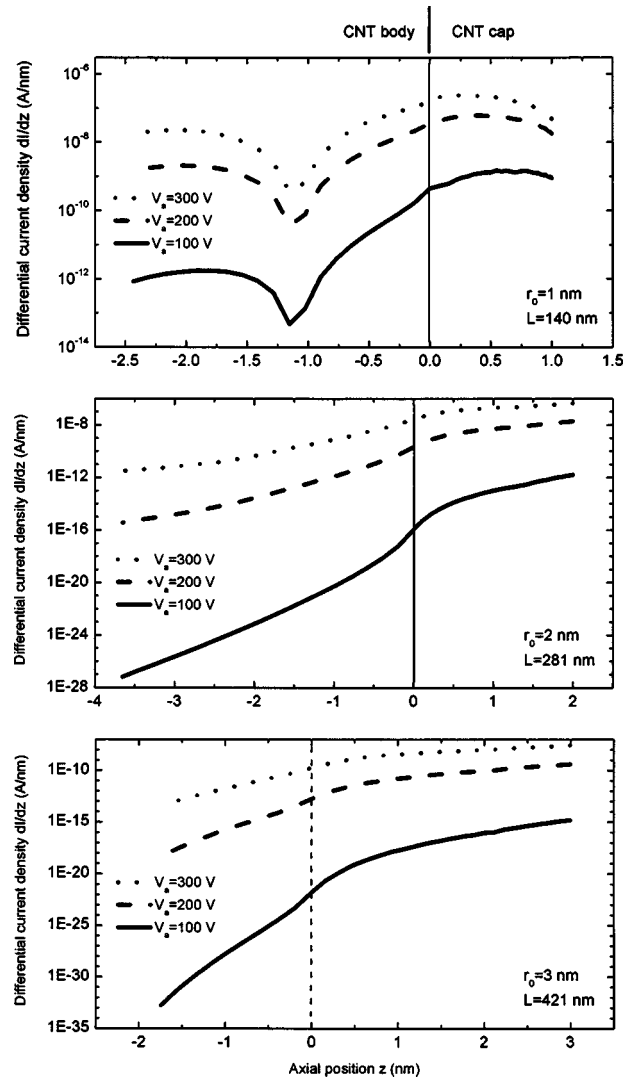


FIG. 7. Axial emission current distributions $dI/d(z)$ for several CNT situations (r_0, L) and applied voltages V_a , for which emission from the CNT apex is allowed to take place.

tion occurs. As the allowed electronic states are strictly determined by the tube dimensions [length and diameter, cf. Eqs. (10) and (11)] and by the substrate boundary condition of Eq. (12), it follows that these configuration parameters and conditions will also determine the axial distribution of the emission current.

One may easily distinguish two different types of CNT configurations: one for which *no electronic state* with vanishing quantum number m is allowed and the other, for which the value $m=0$ is possible. Physically, a nonvanishing value of m means that the electron has a certain amount of axial angular momentum, that is it "rotates" around the z axis and always bears an average lateral "position" on the tube.¹¹ The localization probability at the CNT's tip, at $z=r_0$, vanishes for $m \neq 0$, cf. Eqs. (10), (11), and (13). On the contrary, the localization probability for an electron with $m=0$ is always nonzero. It is then clear that, from the field emission point of view, these two distinct situations imply either vanishing emission from the CNT's tip (when $m=0$ is forbidden)

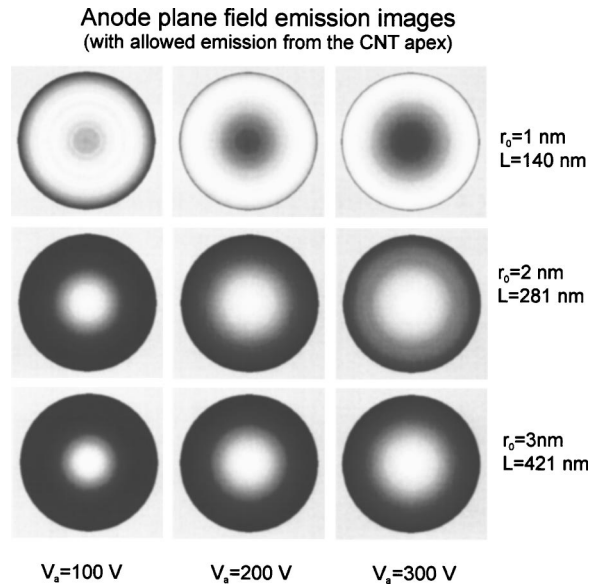


FIG. 8. Anode plane field emission images (with allowed emission from the CNT apex). The images correspond to the current distributions shown in Fig. 7.

or nonvanishing tip emission (when $m=0$ is allowed). These two situations will obviously generate distinct images on the anode: ring images only will appear when $m=0$ is forbidden and central spots, eventually surrounded by rings (of more or less uniform brightness) will be displayed when $m=0$ is allowed.

In order to illustrate the appearance of these two distinct types of field emission images, we have considered two corresponding types of CNT configurations. Thus, for Fig. 7, we chose tube configurations (indicated on the figure) that allow states with $m=0$ and the axial distribution of the emission current is computed for several values of the anode potential. It can be seen that, as suggested in Ref. 11, the differential emission current is far from having a regular behavior on the CNT's cap and body. Non vanishing emission from the tip is found in all these situations.

Taking into account the electron trajectories, also computed with SIMION,¹³ we were able to obtain the related images that should appear on the anode plane. These images, conventionally drawn in grayscale with “white” color attributed to the maximum value of the current density, are shown in Fig. 8. The emission from the tip is visible in almost all images, but in the upper row there is a somehow puzzling behavior: The higher voltage images seem to be actually annular. However, a glance at the related diagrams of Fig. 7 shows that this is not actually the case; there is nonvanishing emission from the tip, but the lateral emission is much more consistent. This situation occurs in very thin tubes, where, along with *possible* states with $m=0$, *more probable* states with $m \neq 0$ and comparable energies are occupied. Thus, under very high extraction fields, such “laterally localized” states will produce more consistent currents than the states “localized” on the tip area.¹¹

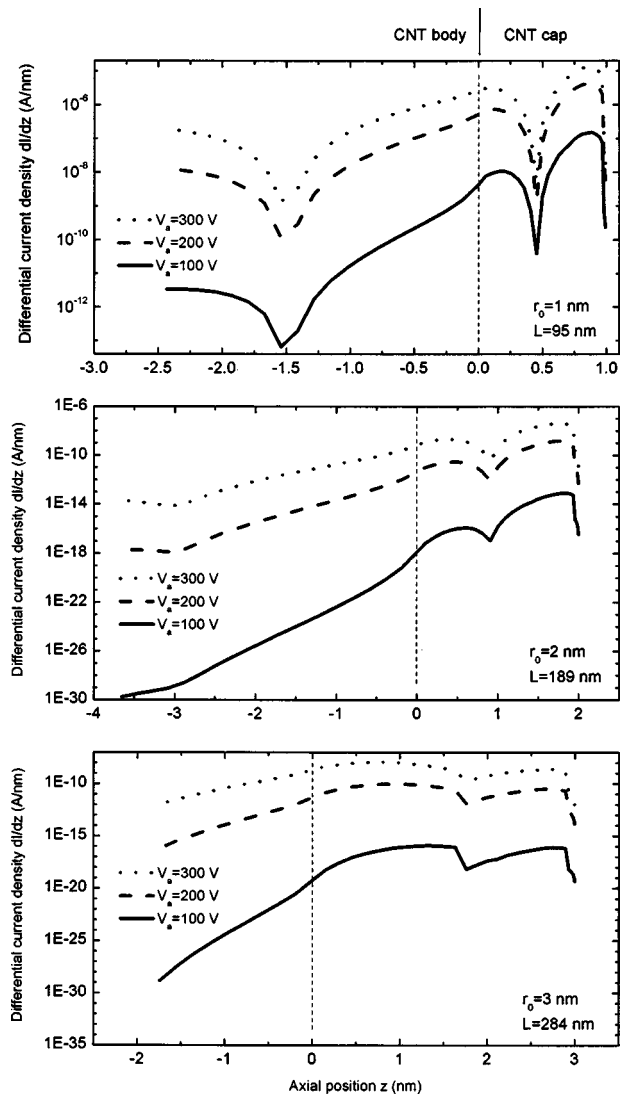


FIG. 9. Axial emission current distributions $dI/d(z)$ for several CNT situations (r_0, L) and applied voltages V_a , for which the emission from the CNT apex is forbidden.

The purely annular type of field emission images is illustrated by the diagrams of Fig. 9 and by the related images of Fig. 10. For these cases, special tube configurations have been chosen, which forbid electronic states with $m=0$. The difference from the previous case is obvious: While the differential emission current is still highly inhomogeneous along the CNT axis, no emission occurs from the tip. As a consequence, very clear annular images should appear on the anode. For thicker tubes, it can be seen that even multiple rings can be obtained. However, in very high extraction fields, these rings coalesce and recede to the outermost part of the image (see the lowest row of Fig. 10).

We may also note that, besides the two major cases illustrated above, one very frequently gets tube configurations for which the axial current distribution is almost zero at any position on the CNT. Such situations appear when the allowed quasifree electronic states have too high energies to be occupied with any significant chance. They may account for

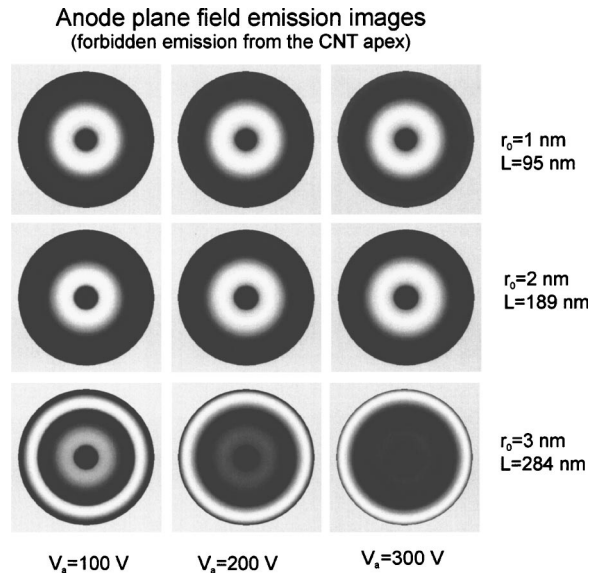


FIG. 10. Anode plane field emission images (with forbidden emission from the CNT apex). The images correspond to the current distributions shown in Fig. 9.

the vast number of CNTs, from usual (even well-aligned) films, which emit no electrons, even at very large anode potentials.

Finally, we observe that, even if very simple, the quasifree electron model can be used as an analytical tool in both clarifying the transport properties of CNTs and developing controlled growth of CNT-based high-brightness field emission cathodes.

V. CONCLUSIONS

A model was constructed in order to describe the behavior of quasifree electrons on a CNT. The CNT was modeled as a continuous two-dimensional manifold comprising a cylindrical body with a hemispherical termination. The quantum constraints imposed by the specific spatial confinement determine the apparition of a specific set of one-particle states for the quasifree electrons. The longitudinal distribution of the quasifree electron density can thus be computed and shown to have spatial periodicity as detected in STM measurements. By applying the same model to a diode configu-

ration of the CNT, the nonhomogeneous extraction field on its surface can be obtained and used to compute the axial distribution of the field emission current. If further boundary conditions are imposed to the other end of the structure (the substrate contact) the model outlines the possibility of inhomogeneous electron field emission for very thin CNTs at high emission levels and the appearance of peculiar ring-shaped and/or spot-shaped field emission images (as well as no-emission situations), in accordance to available experimental observations.

- ¹K. A. Dean, P. von Allmen, and B. R. Chalamala, *J. Vac. Sci. Technol. B* **17**, 1959 (1999).
- ²K. A. Dean and B. R. Chalamala, *J. Vac. Sci. Technol. B* **21**, 868 (2003).
- ³W. Liu, S. Hou, Z. Zhang, G. Zhang, Z. Gu, J. Luo, X. Zhao, and Z. Xue, *Ultramicroscopy* **94**, 175 (2003).
- ⁴Y. Saito, K. Hamaguchi, S. Uemura, K. Uchida, Y. Tasaka, F. Ikazaki, M. Yumura, A. Kasuya, and Y. Nishina, *Appl. Phys. A: Mater. Sci. Process.* **A67**, 95 (1998).
- ⁵W. Zhu, C. Bower, O. Zhou, G. Kochanski, and S. Jin, *Appl. Phys. Lett.* **75**, 873 (1999).
- ⁶J.-M. Bonard, J.-P. Salvetat, T. Stöckli, L. Forró, and A. Châtelain, *Appl. Phys. A: Mater. Sci. Process.* **A69**, 245 (1999).
- ⁷K. A. Dean and B. R. Chalamala, *Appl. Phys. Lett.* **76**, 375 (2000).
- ⁸Y. Saito, K. Hamaguchi, K. Hata, K. Uchida, Y. Tasaka, F. Ikazaki, M. Yumura, S., A. Kasuya, and Y. Nishina, *Nature (London)* **389**, 553 (1997).
- ⁹S. Han and J. Ihm, *Phys. Rev. B* **61**, 9986 (2000).
- ¹⁰A. Mayer, N. M. Miskovsky, and P. H. Cutler, *J. Phys.: Condens. Matter* **15**, R177 (2003).
- ¹¹V. Filip, D. Nicolaescu, M. Tanemura, and F. Okuyama, *J. Vac. Sci. Technol. B* **22**, 1234 (2004).
- ¹²V. Filip, D. Nicolaescu, and F. Okuyama, *J. Vac. Sci. Technol. B* **19**, 1016 (2001).
- ¹³D. A. Dahl, *Simon 3D Version 70. User's Manual*, INEEL-95/0403 (Idaho National Engineering and Environmental Laboratory, Idaho Falls, ID, 2000).
- ¹⁴S. Flügge, *Practical Quantum Mechanics* (Springer, New York, 1974).
- ¹⁵M. Abramowitz and I. A. Stegun, *Handbook of Mathematical Functions* (Dover, New York, 1972).
- ¹⁶A. Hassani, M. Tokumoto, P. Umek, D. Mihailovic, and A. Mrzel, *Appl. Phys. Lett.* **78**, 808 (2001).
- ¹⁷J. W. Gadzuk, *J. Vac. Sci. Technol.* **9**, 591 (1972).
- ¹⁸A. Modinos, *Surf. Sci.* **42**, 205 (1974).
- ¹⁹R. Gomer, *Field Emission and Field Ionization* (Harvard University Press, Cambridge, MA, 1961).
- ²⁰D. Nicolaescu, V. Filip, S. Kanemaru, and J. Itoh, *J. Vac. Sci. Technol. B* **21**, 366 (2003).
- ²¹V. Filip, D. Nicolaescu, M. Tanemura, and F. Okuyama, *Ultramicroscopy* **89**, 39 (2001).